Ramifications of codoping SrI_2:Eu with isovalent and aliovalent impurities

Cite as: J. Appl. Phys. **120**, 213104 (2016); https://doi.org/10.1063/1.4971180
Submitted: 16 October 2016 . Accepted: 17 November 2016 . Published Online: 06 December 2016

Qingguo Feng, and Koushik Biswas

JOURNAL OF APPLIED PHYSICS **120**, 213104 (2016)

Ramifications of codoping SrI_2:Eu with isovalent and aliovalent impurities

Qingguo Feng and Koushik Biswas[a)]
Department of Chemistry and Physics, Arkansas State University, State University, Arkansas 72467, USA

(Received 16 October 2016; accepted 17 November 2016; published online 6 December 2016)

Eu^{2+} doped SrI_2 is an important scintillator having applications in the field of radiation detection. Codoping techniques are often useful to improve the electronic response of such insulators. Using first-principles based approach, we report on the properties of SrI_2:Eu and the influence of codoping with aliovalent (Na, Cs) and isovalent (Mg, Ca, Ba, and Sn) impurities. These codopants do not preferably bind with Eu and are expected to remain as isolated impurities in the SrI_2 host. As isolated defects they display amphoteric behavior having, in most cases, significant ionization energies of the donor and acceptor levels. Furthermore, the acceptor states of Na, Cs, and Mg can bind with I-vacancy forming charge compensated donor-acceptor pairs. Such pairs may also bind additional holes or electrons similar to the isolated defects. Lack of deep-to-shallow behavior upon codoping and its ramifications will be discussed. *Published by AIP Publishing.*
[http://dx.doi.org/10.1063/1.4971180]

I. INTRODUCTION

Eu-doped orthorhombic SrI_2[1,2] and Ce-doped hexagonal $LaBr_3$[3] have recently gained prominence as high-performance scintillators for radiation detection, having superior light yield and energy resolution than other binary halide counterparts,[4] viz., NaI:Tl or CsI:Tl. Notice that the former compounds are structurally more complex than rocksalt or simple cubic structure of the latter materials. Crystalline complexity brings with it several characteristic changes in the electronic and lattice vibrational properties that have been recently deemed to be favorable towards improved luminescence. One clear distinguishing feature that follows from the large 24-atom unit cell in case of SrI_2 is in the electronic band structure, compared to that of the simple 2-atom cell in NaI. Both have dispersive conduction band edge, i.e., low electron effective mass of thermal electrons. But, unlike NaI, the SrI_2 bands above the conduction band minimum (CBM) are flat and dispersion-less (Fig. 1). It has been suggested[5] that this subtle but important distinction may be responsible for limited diffusion of hot electrons owing to their small group velocity and reduced linear quenching via deep traps resulting in proportional and higher light yield in SrI_2. In spite of its advanced features, other metrics such as mechanical properties, ease of crystal growth, decay time, and energy resolution may be improved further in order to remain cost-effective and accommodate the demands of various applications.

Cation site codoping with Group II elements has already proven to be an effective pathway in improving energy resolution of $LaBr_3$:Ce.[6,7] In SrI_2, similar codoping strategies have been attempted with isovalent and aliovalent cations.[8–10] Recent reports suggest degradation in light yield caused by lathanide and alkali metal codopants without any obvious change in scintillation decay time.[8,9] Another study reported on separate samples of SrI_2:Eu, each codoped with a starting 0.2 mole% of Cs, Na, Mg, Ba, Ca, Cu, Fe, or Sn.[10] Among these Na, Ba, Ca, and Sn degraded light yield and energy resolution with the latter having the most harmful effect. The remaining codopants showed good segregation having considerably less concentration in the final crystal and appeared to be benign.[10] In this work, we present a first-principles based density functional study of codoping in SrI_2. We begin with an initial discussion of the host electronic properties and the excitation-emission process involving 4f, 5d orbitals of Eu-activator. It is followed by defect properties of cation site codopants and their impact on the host electronic structure. As isolated impurities all of these codopants are found to induce localized defect levels inside the host band gap, which are likely carrier traps. Codopants having acceptor levels are expected to bind with oppositely charged Iodine vacancy (V_I), similar to the recently described (Sr_{La}-V_{Br}) complex in $LaBr_3$:(Ce, Sr).[11] However, unlike the case of codoped $LaBr_3$, the acceptor-vacancy complex in SrI_2 retain their deep defect-like characteristics and therefore not expected to be beneficial in terms of enhancing its luminescence properties.

II. METHODS AND MODELS

The atomic structure and electronic properties are calculated using density functional theory (DFT) and projector augmented wave method[12] as implemented in the Vienna Ab-initio Simulation Package (VASP).[13,14] We have utilized semilocal (PBE)[15] and hybrid PBE0 exchange-correlation functionals.[16] The semilocal PBE functional, like other generalized gradient approximations (GGA), normally underestimates band gaps in addition to spurious delocalization behavior of certain localized defect systems. Hybrid PBE0 functional which mixes a fraction ($\alpha = 0.25$) of exact Fock exchange, often improves the electronic structure and properties of materials. Using both types of functionals allows us to obtain a perspective on the defect and dopant properties and cross-verify results obtained from one method versus another. Experimentally measured lattice constants, $a = 15.22$ Å, $b = 8.22$ Å, and $c = 7.90$ Å[17] are adopted in all calculations

a)E-mail: kbiswas@astate.edu

while the internal atomic coordinates are relaxed to obtain the optimized geometry of the host crystal. Sampling the Brillouin zone of the 24-atom SrI_2 unit cell using a $4 \times 6 \times 6$ Γ-centered *k*-mesh was found to be adequate for the PBE0 calculations. PBE calculations utilized a finer $8 \times 8 \times 8$ *k*-mesh. An energy cutoff of 250 eV has been used in both types of calculations, while force convergence criteria were set at 0.01 eV/Å and 0.05 eV/Å for PBE and PBE0, respectively. A $1 \times 2 \times 2$ supercell containing 96 atoms is used to simulate defects and dopants in the host. Only Γ-point sampling of the supercell has been performed in PBE0 calculations while the corresponding PBE calculations employed a $2 \times 2 \times 2$ Monkhost-Pack *k*-grid. All presented results are based on PBE0. Sufficiency of the Γ-point only sampling in PBE0 supercell calculations is discussed at the end of Sec. IV, by comparing with relevant results from PBE. We note that the PBE0 functional adequately describe the half-filled Eu $4f^7$ electrons as localized inside the host band gap having identical spin (see details in Sec. III). The empty Eu-f states appear high inside the conduction bands.

III. RESULTS AND DISCUSSION

SrI_2 crystallizes in an orthorhombic structure belonging to the space group Pbca (No. 61). There are two inequivalent iodine sites, labeled as I1 and I2 in Fig. 1(a). I1 is bonded with three and I2 has a more symmetric coordination with four Sr neighbors. Two Sr-I1 bond lengths are about 3.26 Å and another is around 3.39 Å. The four Sr-I2 bonds are within 3.34–3.42 Å. The electronic band structure and density of states (DOS) for SrI_2 has been reported earlier.[5,18–20] Our current calculations are in agreement with previous studies and here we point out only a few salient features. SrI_2 has a wide and direct band gap of about 5.65 eV at the Γ-point obtained with PBE0 functional and experimental lattice parameters (Fig. 1(b)). Recent experimental band gaps lie roughly around this value, estimated to be about 5.85 and 5.5 eV at 10 K and 300 K and in the range 5.7–5.8 eV at 90 K[21,22] Projected DOS shows that the conduction and valence band edge states are primarily derived from Sr 4d and I 5p orbitals, respectively. Semilocal PBE functional predicts an underestimated band gap of about 3.99 eV. However, ground state electronic properties, including the ordering and dispersion of the bands, are adequately described by this functional. The effect of spin-orbit interaction causes splitting in I-5p states and effectively broadens valence band width, reducing the band gap by about 0.3 eV. Heavy-metal halides such as those containing Tl or Pb often undergo significant splitting in the conduction band p-states due to spin-orbit coupling.[23,24] Limited spin-orbit interaction in SrI_2 is not expected to play a major role in its host and defect properties. The flat top of the valence bands is typical of alkali- and alkaline earth halides, signifying prompt localization via self-trapped holes (STH).[25,26] Contrary to the dispersion-less valence band maximum (VBM), parabolic nature of the conduction band minimum (CBM) implies free carrier-like transport of thermal electrons. Perhaps an important characteristic of SrI_2 is observed in the flat conduction bands above CBM owing to its complex unit cell and reduced Brillouin zone – a feature unavailable in traditional NaI/CsI scintillators. As discussed by Li *et al.*,[5] low group velocity of hot electrons prevents them from diffusing too far away from the ionization track and consequently encounters fewer spatially localized deep traps, which works in favor of radiative recombination and proportional light yield.

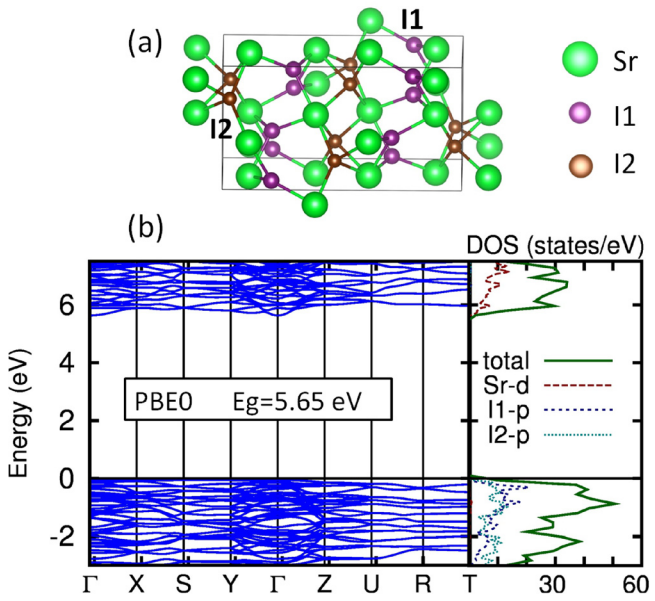

FIG. 1. (a) The crystal structure of SrI_2 in an orthorhombic unit cell. Two distinct iodine sites are shown as I1 and I2. (b) The calculated host band structure and density of states using experimental lattice parameters and PBE0 functional.

A. Eu-doped SrI_2

Isovalent substitution of Eu^{2+} on a Sr^{2+} site is favored in SrI_2 due to their nearly identical ionic sizes[27] and structural similarity with 7-fold coordinated orthorhombic EuI_2.[28] EuI_2 also has a stable monoclinic phase.[29] The calculated DOS show that the localized, half-occupied (high-spin) Eu $4f^7$ orbitals appear inside the band gap of SrI_2 and the Eu 5d orbitals are resonant in the conduction bands near CBM. The gap between Eu 4f and the VBM is about 0.84 eV per our PBE0 calculation which is smaller than the fitted gap of about 1.4 eV deduced by Chaudhry *et al.*[30] Nevertheless, the essential features that enable Eu^{2+} activation is appropriately described, allowing us to qualitatively discuss luminescence in SrI_2:Eu. Figure 2 illustrates the absorption-emission behavior using schematic configuration coordinate diagram and DOS obtained from constrained DFT calculations. The $4f \rightarrow 5d$ optical excitation is modeled following Frank-Condon principle and transferring one Eu-f electron to the lowest d orbital near CBM, keeping ground state geometry. The absorption energy is then given by total energy difference between the ground state and excited configuration, as shown in Fig. 2. It is calculated to be about 4.04 eV which is in reasonable agreement with optical absorption energy around 4 eV.[22,31–33] Next, the lattice re-configures and coupling allows the excited electron to localize on Eu 5d, exposing it inside the band gap and creating the *relaxed-excited* structure (Fig. 2). Emission ensues via 5d-4f recombination.

Our calculated emission energy (~3.71 eV) is larger than typical Eu^{2+} emission of about 2.9 eV.[31–33] This discrepancy is likely due to incomplete localization of the hole and electron that participate to form an excitonic state prior to emission. In any case, this absorption-emission mechanism highlights the importance of Eu as an activator and positioning of its f, d orbitals inside the host gap. If the Eu 5d are energetically too high in the conduction bands or if its f states dip below the host VBM, then luminescence may not be favored, rendering such materials nonscintillators. We have recently discussed the possibility of such circumstances in few other Eu-doped complex halides where an excited electron preferably localizes on the ns^2 ion p-states near CBM while the Eu 5d in the upper conduction bands remain unoccupied.[34]

B. Codoped SrI_2

1. Codopants as isolated impurities

Defects and dopants couple with their local lattice, which may induce shallow or deep donor/acceptor levels inside the host band gap and undergo charge-state transitions via capturing one or more carriers. It is useful to know such thermal (equilibrium) or vertical (optical) transition levels. Formation energy of defects and dopants is another important consideration, because it is related to their relative concentrations under equilibrium. Low formation energy means large concentration of a native defect or high solubility of an impurity which may impact material properties. First-principles methods are an effective tool to estimate defect formation energies and transition levels as briefly discussed below.[35]

The formation of a particular point defect involves changes in the local lattice and exchange of atoms from respective chemical reservoirs that are participating in the process. If the defect captures carriers, i.e., electron/holes, then it also involves changes in the electron chemical potential. All of these can be formulated into the formation energy of a defect D in charge state q, as

$$\Delta H(D,q) = (E_D - E_{host}) - \sum_i n_i(\mu_i^{el} + \Delta\mu_i) + q(E_V + E_f) + E_{corr}. \quad (1)$$

Here, the first term is the difference in total energy between the host and defect-containing supercell calculation. It accounts for the lattice relaxation and charge redistribution caused by the defect. Second term is the atomic chemical potential term, representing the energy associated with the exchange of atoms necessary to create the defect. Change in energy due to exchange of electrons or holes in a charged defect is accounted in the third term, where E_V is the energy at VBM of the defect-free host. E_f, which is often referred as the Fermi energy in this context, is a parameter whose value spans the entire band gap from VBM to CBM. Note that this term is applicable only for charged defects ($q \neq 0$) and can substantially affect the formation energy. The last term E_{corr} in Eq. (1) is a correction term introduced to remedy the anomalies caused by finite size of a defect supercell calculation which does not properly reflect dilute limits. There are two major contributions to E_{corr}: one is aligning the average potential of a charged defect supercell and the unperturbed host and the other is spurious electrostatic interaction between the charged defect and its periodic images. Inaccuracies in ΔH are also introduced due to band gap error of semilocal density functionals affecting E_V and E_f. Improper accounting of these contributions may have a bearing upon the defect physics of a particular system. Once the formation energies of a defect in its possible charge states are calculated, the equilibrium transition level is given by: $\varepsilon(q_1/q_2) = \frac{\Delta H(D,q_1) - \Delta H(D,q_2)}{q_2 - q_1} - E_V$. It gives the value of E_f when $\Delta H(D,q_1) = \Delta H(D,q_2)$. Again, incorrect band edges caused by the "band gap problem" may render a deep level appear shallow.

Unlike Eu which is easily incorporated without considerable relaxation of the SrI_2 lattice, other isovalent or aliovalent codopants may induce defect structures that can affect the electronic properties of the host. We have earlier reported on the formation of defect complex ($Tl_{Na} + Ca_{Na}$) in codoped NaI:(Tl, Ca).[36] In case of codoped SrI_2:(Eu, X) [X = Mg, Ba, Ca, Sn, Cs, Na], there is no significant dopant-codopant interaction, and the calculated ($Eu_{Sr} + X_{Sr}$) binding energies are all positive values within a few (tens of) meVs. Note that we define binding energy as the difference between formation energy of a complex and that of the respective isolated dopants, i.e., $E_b(\mathrm{Eu} + \mathrm{X}) = \Delta H_{\mathrm{Eu+X}} - \Delta H_{\mathrm{Eu}} - \Delta H_{\mathrm{X}}$. Therefore, only negative values of E_b imply dopant-codopant binding. It is an interesting contrast with NaI:(Tl, Ca) where we found evidence of Tl-Ca dimer formation that transforms the shallow donor level of isolated Ca^{2+} to a deep DX-like acceptor.[36] Subsequent experiments suggested that this Tl-Ca pairing may be partially responsible in removing slow decay component and improve the energy resolution and scintillation decay time of codoped NaI.[37,38] In case of SrI_2, we infer that the chosen codopants do not preferentially bind with Eu; however, they may still affect electronic properties of the host as isolated impurities. Hereafter, we discuss these codopants as isolated defects in SrI_2.

In defect nomenclature, a substitution at Sr-site is considered a charge-neutral defect. Hence isovalent Ba^{2+}, Ca^{2+}, Mg^{2+}, or Sn^{2+} substituting at Sr^{2+} are the neutral charge states of the respective defects (Ba^0_{Sr}, Ca^0_{Sr}, Mg^0_{Sr}, Sn^0_{Sr}). These neutral defects may become positively or negatively charged via hole or electron capture. Similarly, a monovalent Cs^+ or Na^+ substituting at Sr^{2+} is referred as Cs^0_{Sr} and Na^0_{Sr}, respectively. Nominally, they are acceptor defects and may appear as Cs^-_{Sr} or Na^-_{Sr} after capturing an electron. It is important to ascertain the defect levels and ionization energies of these codopants. We proceed by evaluating the formation energies of various codopants and the I-vacancy defect (V_I), which are germane to our discussion. The term $(\mu_i^{el} + \Delta\mu_i)$ in Eq. (1) represents the chemical potential $\Delta\mu_i$ of an atom "i" relative to its elemental bulk state μ_i^{el}. For accurate calculation of ΔH, we must then find the ranges, $\Delta\mu_i$ of each codopant that permits its formation within SrI_2, and without the possibility of forming any other secondary phases such as MgI_2, BaI_2, CaI_2, SnI_2, SnI_4, CsI, and NaI. Those requirements and calculated formation enthalpies of relevant phases are given in the Appendix.

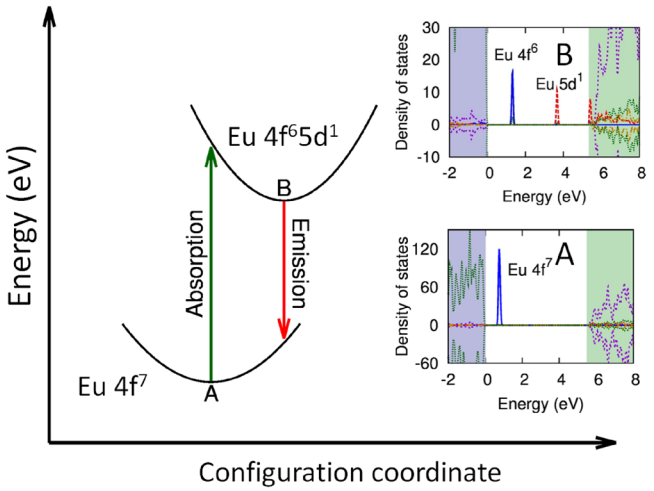

FIG. 2. Schematic configuration coordinate diagram showing Eu 4f-5d transition in SrI_2. Density of states plot illustrate the ground state Eu $4f^7$ marked "A" and the *relaxed-excited* $4f^6 5d^1$ configuration as "B."

Figure 3 shows the calculated formation energies of different codopants. Since there is a possible excursion in the achievable values of $\Delta\mu_i$, we show them under I-rich and Sr-rich conditions which serve as their limits within which all values are possible. The slopes of these lines refer to the preferred charge state of an impurity or defect under equilibrium. A change of slope represents the transition level and gives the value of E_f when one charge state is thermodynamically stable over another.

Substitutional Ba^0_{Sr} does not induce any localized level within the host gap, and there is no significant lattice relaxation. It is due to the chemical and structural similarities of SrI_2 and BaI_2 and both of them are known scintillation host materials. The average Ba-I bond length is about 3.46 Å, slightly larger than those of Sr-I (3.34 Å), due to larger ionic radius of Ba^{2+}. However, the singly charged defect, i.e., Ba^+_{Sr} and Ba^-_{Sr} respectively induce localized hole and electron state, which is reflected in the formation energy plot shown in Fig. 3. The $\varepsilon(+/0) = 0.25$ eV and $\varepsilon(0/-) = 5.52$ eV transition levels are relatively shallow compared to other

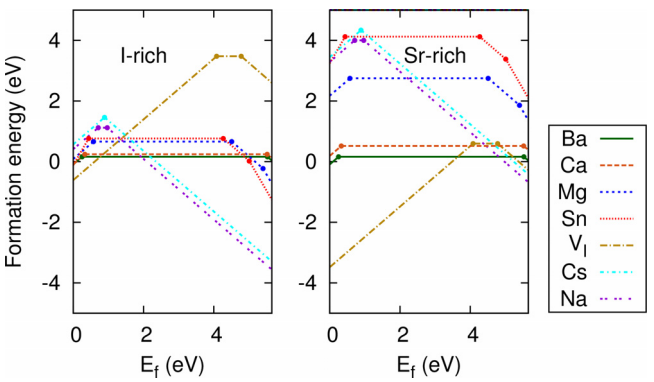

FIG. 3. Calculated formation energy and charge transition levels of codopants and the native I-vacancy appearing as isolated defects in SrI_2. The values are shown at I-rich and Sr-rich conditions. Formation energies are depicted as function of E_f which span the band gap from VBM ($E_f = 0$ eV) to CBM ($E_f = 5.65$ eV). The slopes (+2, +1, 0, − 1, − 2) of each line refer to the stable charge state of a defect and change in slope represents equilibrium transition level.

codopants. Note that all the transition levels discussed here are referenced with respect to host VBM, E_V. The neutral charge state has low formation energy of 0.16 eV under both I-rich and Sr-rich limits and remains thermodynamically stable in the majority of the band gap. In the same vein, substitutional Ca^0_{Sr} also has low formation energy (0.24 eV, I-rich and 0.52 eV, Sr-rich) with +/0 and 0/– transitions at 0.33 eV and 5.52 eV above E_V. Low formation energies in either case reveal that these codopants are freely soluble within SrI_2. We should point out that PBE calculations predict delocalized solutions in Ba^+_{Sr}, Ca^+_{Sr} (holes at VBM) and Ba^-_{Sr}, Ca^-_{Sr} (electrons at CBM), respectively. It is due to inherent bias of GGA functionals towards shallow behavior, which we shall revisit again while discussing Na, Cs codopants.

Unlike the previous two codopants, Mg^0_{Sr} induces an unoccupied deep level inside the host bandgap. The Mg 3s single-particle level appears 0.62 eV below CBM (Fig. 4), accompanied with a relaxation of the local lattice. Mg^{2+} strongly bonds with five surrounding I-ions, moving almost to an interstitial position—reminiscent of a vacancy-interstitial Frenkel pair. Five Mg-I bonds are considerably shorter, around 2.92 Å constructing a quasi-octahedral structure, while the remaining two I-neighbors move afar with an average distance of about 4.12 Å (Fig. 4). It is due to large differences in cation-anion size. This configuration may be compared with hexagonal structure of MgI_2 where the Mg cations occupy octahedral sites in alternating layers having Mg-I bond length of 2.92 Å.[39] The deep Mg-s level in Mg^0_{Sr}

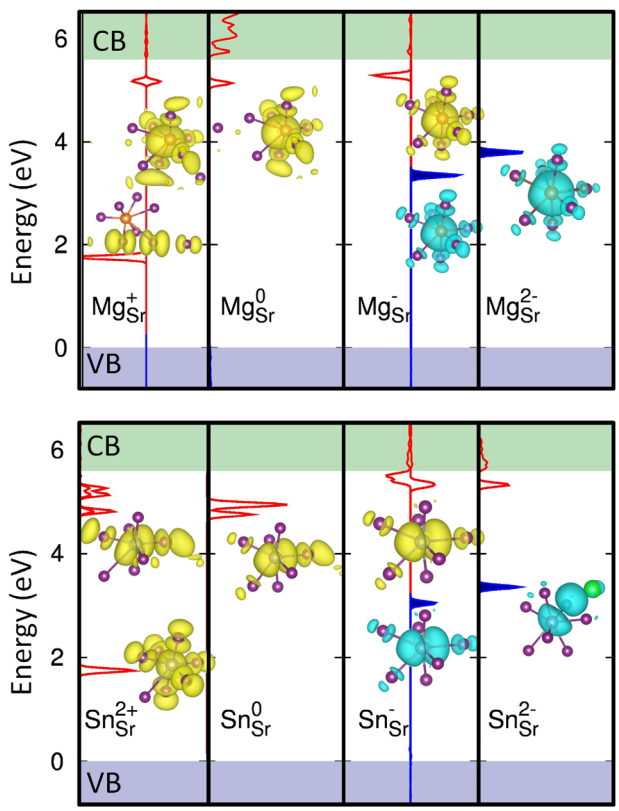

FIG. 4. Localized gap levels and isosurface corresponding to different charge states of isolated Mg and Sn in SrI_2. Spin up/down channels are shown in case of spin-polarized calculations. Solid peaks and blue isosurface signify occupied levels.

may trap electrons transforming to Mg_{Sr}^{-} and Mg_{Sr}^{2-}. After capturing electrons, the ionic radius ratio between Mg and I increases and the lattice rearranges when the dopant ion recedes from interstitial towards ideal site. Now the p-states of all seven I-neighbors hybridize with the occupied Mg s^2 orbital, sharing the localized electrons and having an overall bond length of 3.56 Å in Mg_{Sr}^{2-} (Fig. 4). In the I-rich limit Mg_{Sr}^{0} has low formation energy of 0.67 eV and increases to 2.75 eV in the Sr-rich case. Fig. 3 shows deep 0/– and –/2– levels at 4.51 eV and 5.40 eV above the VBM, respectively. In addition to its neutral and negatively charged acceptor states, Mg_{Sr}^{+} is also stable inside the gap with its (+/0) level located 0.58 eV above VBM. This hole state is similar to Ca_{Sr}^{+} where the hole is captured at two neighboring iodines as in a I_2^- molecular ion.

Sn_{Sr}^{0} represents the +2 valence state of Sn substituting at Sr^{2+}. It distorts the lattice in a similar fashion as Mg_{Sr}^{0}, binding strongly with five nearest iodine neighbors having bond lengths ~3.1 to 3.3 Å and remaining two at ~3.6 Å. The DOS peak (Fig. 4) appearing below CBM is unoccupied and primarily Sn 5p, hybridized with I 5p states. These localized levels below the CBM may also act as electron traps. Upon capturing an electron Sn_{Sr}^{-} forms a trigonal prism-like structure with four stretched Sn-I bonds ~3.6 Å in length and the other two ~3.06 Å. There is a seventh I^- neighbor ~3.94 Å apart. In Fig. 4, Sn_{Sr}^{-} appears as a partially occupied state deep inside the band gap, comprising of Sn-p and I-p. After capturing one additional electron the Sn_{Sr}^{2-} deep level is fully occupied. The local lattice tends towards a distorted tetrahedral structure having two iodine neighbors at ~3.10 Å and the other two at ~3.48 and 3.76 Å, respectively. Due to the localization of two electrons at Sn, there is an additional Sn-Sr cation bond of ~3.46 Å and the gap state comprise of Sn, I p along with admixture of Sr d orbitals.

The nominally inert Sn $5s^2$ carrying the lone pair has its antibonding orbitals near the host VBM. After capturing holes it moves inside the gap as Sn_{Sr}^{2+} (Fig. 4). This charge state of Sn is possible due to its ability to change valency from Sn^{2+} to Sn^{4+} via hole capture (or donating its lone pair). In defect nomenclature it is denoted as Sn_{Sr}^{2+} ($Sn_{Sr}^{0} + 2h \rightarrow Sn_{Sr}^{2+}$). In effect, it is the multivalent tendency often found in lead or stannous halides and chalcogenides. The divalent Sn^{2+} reaching a higher oxidation state of Sn^{4+} is of interest from a defect perspective because of its inherent capacity to act as an electrically active center, influencing the behavior of excited charge carriers. Sn_{Sr}^{2+} forms an octrahedral coordination with six anion neighbors having Sn-I average bond lengths ~2.95 Å. The lone pair of Sn_{Sr}^{0} that appeared as a perturbation in the host valence band is now emptied and the hole state consisting Sn 5s is located almost 1.9 eV above the VBM (Fig. 4). The empty Sn 5p states remain inside the gap, below CBM. This activity of the lone pair and the appearance of s, p gap states will have additional repercussions on Sn codoped SrI_2 (see Sec. IV).

Similar to the prior isovalent codopants, Sn_{Sr}^{0} has low formation energy of 0.77 eV in the I-rich limit. In the Sr-rich regime it is much larger, about 4.12 eV (Fig. 3). We see the deep double donor transition $\varepsilon(2+/0) = 0.44$ eV, resulting from the multivalent character of Sn. The acceptor transitions corresponding to Sn_{Sr}^{-} and Sn_{Sr}^{2-} lie higher in the host gap at $\varepsilon(0/-) = 4.27$ eV and $\varepsilon(-/2-) = 5.0$ eV, caused by occupation of Sn 5p levels below the CBM.

Cs^+ and Na^+ are aliovalent codopants and when substituting at Sr^{2+} they are represented as Cs_{Sr}^{0} and Na_{Sr}^{0}, respectively. It corresponds to a hole state which can transition to a singly charged acceptor state, i.e., Cs_{Sr}^{-} or Na_{Sr}^{-}. Both codopants create less deformation of the local lattice compared to isovalent Mg or Sn. Due to its larger ionic radius the Cs-I bonds in Cs_{Sr}^{0} are on average longer (~3.67 Å) than the corresponding Na-I bonds (~3.31 Å), whereas the median value of Sr-I distances in the host is about 3.34 Å. Even without large lattice relaxation both are deep acceptors, meaning Cs_{Sr}^{0} and Na_{Sr}^{0} are localized holes at adjacent iodine neighbors. The hole state is composed of partially occupied I 5p which can trap one additional hole (e.g., $Cs_{Sr}^{0} + h \rightarrow Cs_{Sr}^{+}$). It is perhaps not surprising given the propensity of the iodine lattice to trap holes. We note that the hole capture adjacent to these aliovalent codopants is not entirely identical, possibly caused by differences in cation sizes. In Cs_{Sr}^{+} the two holes are localized between first and second nearest iodines, while in Na_{Sr}^{+} both holes are shared between two nearest iodines (Fig. 5). It is similar to V_k-like configuration where the iodines sharing the hole tend towards a molecular ion, coming within about 3.3 Å in Cs_{Sr}^{+} and 2.7 Å in Na_{Sr}^{+}, compared to an undistorted I-I distance of 3.96 Å. Figure 3 shows the Cs_{Sr}^{+} and Cs_{Sr}^{-} are stable under equilibrium with double acceptor transition: $\varepsilon(+/-) = 0.89$ eV, while Cs_{Sr}^{0} remains metastable. In case of Na, there is only a small range of E_f when Na_{Sr}^{0} is thermodynamically stable. It is notable that both Cs and Na create deep hole states in SrI_2 which is unlike the shallow Sr_{La} level found in codoped $LaBr_3$:(Ce, Sr).[11]

We note that PBE calculation favors a delocalized solution and the hole is found to be shallow which we believe is an artifact of the residual self-interaction caused by semilocal approximation of the exchange energy. It is of interest that in hybrid functional PBE0 calculation the electron addition energy ($Cs_{Sr}^{0} + e \rightarrow Cs_{Sr}^{-}$) is close to the energy eigenvalue of the initial unoccupied level, in accordance with Koopman's theorem.[40] Thus, unlike PBE, PBE0 restores linearity of the energy with respect to occupation and correctly predicts a localized hole solution.

2. Codopant—vacancy (X_{Sr}-V_I) complex

Apart from the substitutional dopants, F-centers are well-known defects in halide crystals. A few reports already exist on the donor-acceptor levels of I-vacancy (V_I) in SrI_2.[33,41] We briefly discuss our V_I results before mentioning codopant-V_I complex. There are two possible vacancy sites and both induce deep levels. Our supercell approach shows that the vacancy at I2 site (V_{I2}) is lower in energy by about 0.13 eV than the corresponding I1-vacancy. The symmetric 4-fold coordination available at I2 likely stabilizes this vacancy. It is an a1-like deep donor state created by hybridization of the four host cation dangling bonds, inducing a single-particle level below CBM. The average Sr-Sr separation changes from 5.45 Å in the host lattice to 5.86 Å in V_{I2}^{+} (F^+), 5.35 Å in V_{I2}^{0} (F^0), and 4.84 Å in V_{I2}^{-} (F^-). Trapping

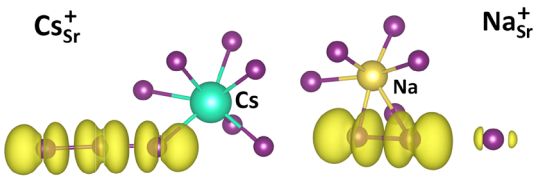

FIG. 5. A comparison of localized hole state induced by Cs^{+}_{Sr} and Na^{+}_{Sr} in SrI_2.

one or two electrons causes an inward relaxation of the surrounding Sr ions toward the vacancy due to increased hybridization and lowers the occupied level further inside the gap. Figure 3 shows all three charge states of V_{I2} are thermodynamically stable. It is similar to electron trapping at anion vacancies found in large gap alkali halides. Our calculated equilibrium transition levels [$\varepsilon(+/0) = 4.08$ eV and $\varepsilon(0/-) = 4.78$ eV] are in qualitative agreement with a previous calculation[41] and estimated thermoluminescence trap depth of 1.12–1.13 eV.[33] However, this deep trapping behavior differs from few other materials of interest, such as the shallow halogen vacancies found in TlBr, $CH_3NH_3PbI_3$ or a negative-U-like direct (+/–) transition close to the CBM seen in $CsPbBr_3$. Shi and Du recently discussed about these possibilities and shallow versus deep behavior of halogen vacancies.[42] Compared to these compounds, lower symmetry of I-vacancy in SrI_2 allows hybridization of the cation dangling bonds and exposes them inside the large band gap, enabling it to act as deep trap instead of remaining shallow.

The deep donor character of V_I^+ may create the possibility of forming codopant-vacancy complex via attractive Coulomb interaction with acceptor defects such as Mg^-_{Sr}, Na^-_{Sr}, or Cs^-_{Sr}. Indeed, we find substantial binding energies of charge-compensated neutral complexes formed between the acceptor states of codopants and V_I^+ (Table I). Sn has been already reported as harmful dopant[10] and hence not included in this discussion, although it also binds with V_I^+. Ba and Ca prefer to retain their neutral charge state through most of the band gap (Fig. 3) and binding with V_I^+ may not be favored. $(Mg_{Sr}–V_I)^0$ may be thought of as pairing between Mg^-_{Sr} and V_I^+. Figure 6 reveals that $(Mg_{Sr}–V_I)^0$ is not thermodynamically stable. The weakly bound positively charged complex between Mg^0_{Sr} and V_I^+ has a negative-U behavior where it captures two electrons with transition level: $\varepsilon(+/–) = 3.7$ eV. The localized levels of $(Mg\text{-}V_I)^+$ are similar to isolated Mg^0_{Sr} (deep Mg-s state) and V_I^+ (deep Sr dangling bond state). The transition to $(Mg_{Sr}–V_I)^-$ occurs when the Mg moves to an interstitial position close to original I-vacancy site, leaving behind a cation vacancy via, $(Mg_{Sr}–V_I)^+ + 2e \rightarrow (Mg_i + V_{Sr} + V_I)^-$. Notice the dominant spherical Mg-s character of this doubly occupied gap state interacting with surrounding I-p and Sr-d shown in Fig. 7. It is a Frenkel-like combination of a Mg-interstitial with V_{Sr} and V_I. In addition to this defect level, there are empty gap states formed by the dangling bonds corresponding to V_{Sr} and V_I (Fig. 7).

TABLE I. Binding energies of neutral codopant-vacancy complex, $E_b(X_{Sr} + V_I) = \Delta H_{X_{Sr}+V_I} - \Delta H_{X_{Sr}} - \Delta H_{V_I}$. Values are given for complex with I1-vacancy (V_{I1}).

Defect system	Binding energies (eV)
SrI_2:($Mg_{Sr} + V_{I1}$)	−0.497
SrI_2:($Sn_{Sr} + V_{I1}$)	−1.101
SrI_2:($Cs_{Sr} + V_{I1}$)	−4.102
SrI_2:($Na_{Sr} + V_{I1}$)	−3.952

$(Cs_{Sr}–V_I)$ and $(Na_{Sr}–V_I)$ complexes also have multiple stable charge states as depicted in Figure 6. The $(Cs_{Sr}–V_I)^0$ and $(Na_{Sr}–V_I)^0$ are formed by pairing between Cs^-_{Sr}, Na^-_{Sr}, and V_I^+, resulting in an overall charge neutral complex. This characterization instead of a simple $(Cs^0_{Sr}–V^0_I)$ [or $(Na^0_{Sr}–V^0_I)$] dimer is evident from a comparison of the induced defect levels shown in Fig. 8. The localized hole state of Cs^0_{Sr}, present in $(Cs_{Sr}–V_I)^+$, recedes inside the VBM after capturing an electron forming $(Cs_{Sr}–V_I)^0$ [$\varepsilon(+/0) = 0.39$ eV], leaving the empty state of V_I^+ intact within the gap. The same is true for $(Na_{Sr}–V_I)$ which has a transition level $\varepsilon(+/0) = 0.44$ eV. In each of the different charge states of the complex, the localized defect levels appear at similar energies when compared to those of participating isolated defects. It means that the carrier capture mechanisms via deep levels discussed earlier in the context of isolated codopants and V_I are still operational in case of these complexes.

Recent first-principles calculations in case of codoped $LaBr_3$:(Ce, Sr),[11] have shown that attractive Coulomb interaction between oppositely charged Sr^-_{La} and V^+_{Br} leads to the formation of a shallow neutral complex $(Sr^-_{La} + V^+_{Br})$. The formation of such a complex may potentially eliminate deep traps induced by V_{Br}, and help the sequential hole and electron capture at Ce^{3+}. Therefore, codoping with Sr facilitates Ce^{3+} activated scintillation in $LaBr_3$ via fast trapping/detrapping of electrons at the shallow complex, which reduces carrier loss via Auger and bimolecular recombination. In case of SrI_2:(Eu, Cs) and SrI_2:(Eu, Na), the induced levels of $(Cs_{Sr}–V_I)$ or $(Na_{Sr}–V_I)$ are deep, similar to those of the isolated defects and expected to remain as active charge traps. We may surmise that the benefit of deep-to-shallow behavior observed in $LaBr_3$:(Ce, Sr) may not be available in SrI_2:Eu when codoped with acceptor impurities like Na or Cs.

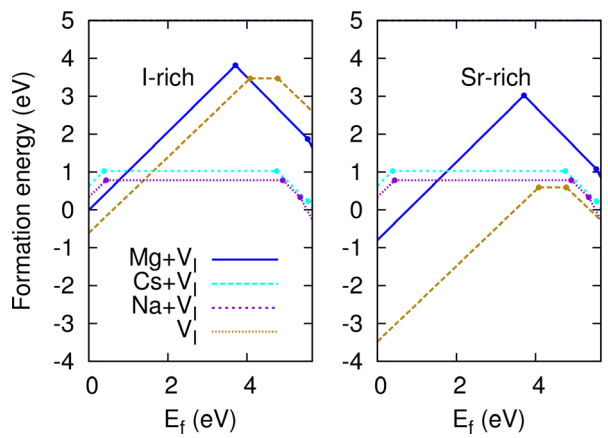

FIG. 6. Calculated formation energy and charge transition levels of codopant-vacancy complex in SrI_2. The values are shown at I-rich and Sr-rich conditions. Formation energies are depicted as function of E_f which span the band gap from VBM ($E_f = 0$ eV) to CBM ($E_f = 5.65$ eV). The line-slopes refer to the stable charge state of a complex under equilibrium while a change in slope marks a transition level.

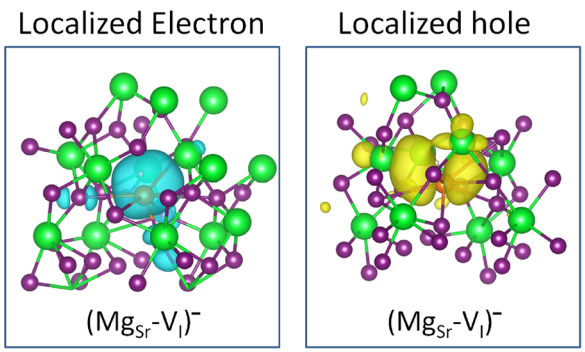

FIG. 7. The dominant Mg s-character of the occupied gap state and the empty hole state formed by Sr and I dangling bonds in $(Mg_{Sr}\text{-}V_I)^-$ complex.

IV. SUMMARY

Efficient detection and identification of unknown radioactive sources in an operationally diverse environment requires high spectroscopic resolution of gamma-ray energies. NaI and CsI based scintillators have remained as the work-horse of such detectors, despite their limited energy resolution and light yield. SrI_2:Eu recently entered the arena of commercially available scintillators due to its excellent light yield and energy resolution. However, nuclear security and nonproliferation applications impose even more stringent requirements on energy resolution without compromising on light yield, which then will be ideal to replace more expensive semiconductor detectors. Codoping in SrI_2 is a viable strategy towards this end, especially when one considers the recent successes involving $LaBr_3$.

As highlighted in previous models,[5,19,43,44] light yield nonproportionality of a scintillator is intertwined with the dynamics between free and localized carriers and their arrival and recombination at activator centers versus annihilation across quenching pathways. Expounded further in terms of hot and thermalized carrier transport, it was shown that low group velocity due to non-dispersive upper conduction bands and free carrier-like transport of thermal electrons at the dispersive CBM prevents linear quenching via deep traps in SrI_2.[5] It favors light yield and proportionality in SrI_2. Eu-doping up to 3% showed a remarkably fast decay (subpicosecond timescale) of excitation-induced free carrier and STE absorption.[45] The reason is speculated to be due to expedited transfer of the excitation via capture at Eu^{2+} which has larger solubility and less segregation compared to CsI:Tl, adding to the light yield of SrI_2:Eu. The dispersive CBM of SrI_2 (Fig. 1) is unlike multi-cation halides, e.g., elpasolites (Cs_2LiYCl_6) whose flat CBMs are typically detached from upper conduction bands and promote formation of electron polarons.[46] In SrI_2 the thermal electrons remain free to recombine with STH at Eu^{2+}. All of these properties inherent to SrI_2 are believed to be the factors that influence its improved performance. One recent report based on molecular dynamics simulations show STHs having unexpectedly small migration barriers in SrI_2 at room temperature, which may be another factor favoring luminescence.[47]

Codoping SrI_2:Eu can add to its desirable metrics by playing the role of beneficial defects, suppressing deep levels and/or creating shallow impurity bands that prevent loss mechanisms via nonradiative processes. Indeed, in case of codoped $LaBr_3$:(Ce, Sr) such a methodology has been proposed where the deep bromine vacancy (V_{Br}) transforms to a shallow ($Sr_{La}\text{-}V_{Br}$) complex. If defects are shallow, they appear as a perturbation of the host states and any captured carrier is only bound through a screened Coulomb potential. In such case, they are able to move as band carriers before capture at an activator level. A defect state created deep inside the band gap behaves differently, where a carrier may become trapped for longer time scales due to its localized wavefunction and generally recombine through nonradiative processes. Our current study involving isovalent Mg, Ca, Ba, Sn and aliovalent Na, Cs cations illustrate: (i) there is no preferential Eu-codopant binding, (ii) all codopants appearing as isolated defects induce deep levels serving as potential trap centers, (iii) V_I as a deep donor is expected to be an electron trap and, (iv) considerable binding between acceptor-like codopants and V_I^+ form acceptor-vacancy complex, however, without any deep-to-shallow behavior.

The absence of any binding interaction between Eu and codopant may be an indicator that they prefer to remain as isolated impurities. It is remarkable that all isovalent (Mg_{Sr}, Ba_{Sr}, Ca_{Sr}, Sn_{Sr}) and aliovalent substitutions (Na_{Sr}, Cs_{Sr}) show amphoteric behavior having both donor and acceptor levels inside the host band gap (Fig. 3). Heavier substitutions and ionic size matching appear to dissuade large lattice relaxation. Since the trap levels of Ba_{Sr} and Ca_{Sr} are much shallower than Mg_{Sr} or Sn_{Sr}, within a few tenths of an eV from VBM and CBM, they may act as temporary trapping-detrapping centers which may be the reason for slightly enhanced light yield observed in such samples by Lam *et al.*[10] However, they also observed degraded energy resolution in thicker cylindrical samples of Ba or Ca codoped SrI_2:Eu. Substitutional Mg^{2+}, due to its size mismatch, moves from its ideal lattice position forming a Frenkel-like vacancy-interstitial pair exposing Mg 3s level inside the gap which behaves as a deep acceptor.

The detrimental behavior observed upon Sn codoping may be a consequence of its self-induced change in oxidation state $Sn^{+2} \leftrightarrow Sn^{+4}$, as seen from the deep $\varepsilon(+2/0)$ double donor transition in Fig. 3. Sn^{4+} corresponds to the emptied lone pair when its 5s appears inside the gap in addition to deep 5p state. This raises a scenario where sequential hole capture at Sn 5s and electron capture at Sn 5p may cause 5p-5s emission from Sn centers in SrI_2:(Eu, Sn). A secondary emission peak observed around 600 nm in codoped samples of SrI_2:(Eu, Sn)[10] may be related to this mechanism.

Codoping with Na or Cs induce deep acceptors which is also problematic. The hole states attributed to Na_{Sr}^+ and Cs_{Sr}^+ have ionization energies close to 1 eV which will affect STH transfer to Eu activators. Perhaps, more importantly, their tendency to form a complex with V_I^+ will determine their behavior as codopants. V_I^+ are abundant in SrI_2 as evident from its formation energy plot (Fig. 3) and it is expected to form a complex with Na_{Sr}^- and Cs_{Sr}^- owing to large binding energy caused by Coulomb attraction. While the neutral complex does not scatter charge carriers, it is still an active trap created by the Sr dangling bonds. Furthermore, the deep

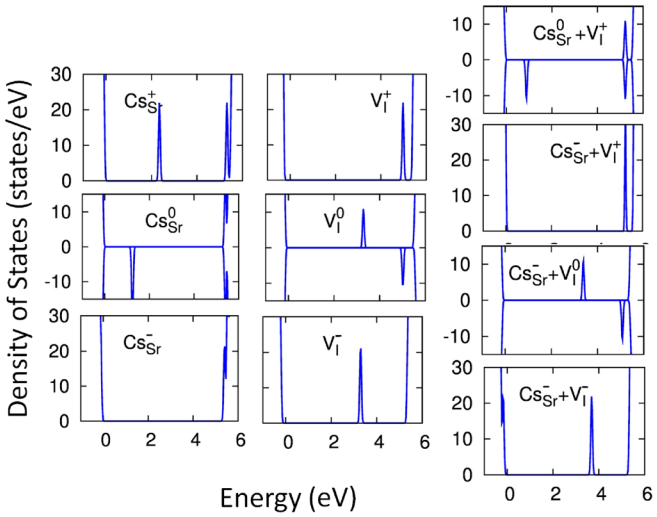

FIG. 8. A comparison between the gap levels created by the four charge states of (Cs_{Sr}-V_I) and those of the isolated defects that combine to from the complex.

levels of each of the constituents, i.e., Cs_{Sr} or Na_{Sr} and V_I remain essentially unperturbed after their association as a complex. As a result all trap levels of the individual defects remain active in the complex form as seen from the multiple donor-acceptor transitions in Fig. 6. Thus the shallow behavior of (Sr_{La}-V_{Br}) complex found in aliovalent codoping of $LaBr_3$:(Ce, Sr) is absent in our Na or Cs codoped SrI_2:Eu. The same can be said about (Mg_{Sr}-V_I) complex which also induce multiple deep levels shown in Fig. 6 corresponding to occupation of the gap states created by its constituent defects.

We end our discussion with a comparative look between defect levels obtained from semilocal PBE and hybrid PBE0 functionals. PBE is a known sufferer from band gap problem and sometimes spurious delocalization behavior of defect localized states. The first drawback is reflected in the underestimated band gap of 3.99 eV. The latter concern is confirmed when PBE arrives at delocalized behaviors of Ba^{+}_{Sr}, Ca^{+}_{Sr}, Ba^{-}_{Sr}, Ca^{-}_{Sr}, Na^{0}_{Sr}, and Cs^{0}_{Sr}, contrary to the localized solutions found in PBE0 calculations. With these exceptions, we wish to illustrate that in other cases PBE gives acceptable results, provided necessary corrections are appropriately implemented. Figure 9 shows a comparison of PBE0 defect levels of codopants and V_I appearing as isolated impurities in SrI_2 with those from PBE (Ba_{Sr}, Ca_{Sr}, Na_{Sr}, and Cs_{Sr} are excluded). The PBE0 band gap is recovered by aligning the average electrostatic potential in the bulk and applying the relative shifts ΔE_v and ΔE_c to the VBM and CBM of PBE, respectively. All selected cases are in good agreement with PBE0 after applying appropriate band-edge shifts relative to PBE0 and potential alignment and image charge corrections in case of charged defects (in accordance with modified Makov-Payne correction of Lany and Zunger in Refs. 48 and 49). It also serves as a reaffirmation of the PBE0 results obtained from "Γ-point only" sampling of the supercell, while those from PBE were obtained using larger $2 \times 2 \times 2$ Monkhorst Pack k-mesh, all other parameters remaining same.

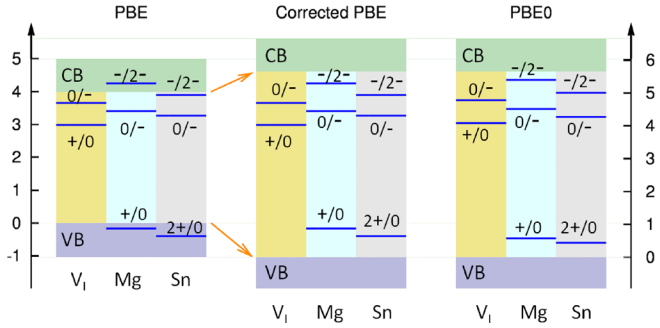

FIG. 9. Comparison of defect levels of selected codopants and I-vacancy obtained from PBE, corrected-PBE, and PBE0 calculations.

ACKNOWLEDGMENTS

This material is based upon work supported by the U.S. Department of Homeland Security under Grant Award Number, 2014-DN-077-ARI075-04. The support does not constitute an express or implied endorsement on the part of the Government. This research used resources of the National Energy Research Scientific Computing Center, which was supported by the Office of Science of the U.S. Department of Energy under Contract No. DE-AC02-05CH11231. Computational resources at Arkansas State are partially funded from NSF Grant No. ECCS-1348341.

APPENDIX: CALCULATION OF EQUILIBRIUM CHEMICAL POTENTIALS

The second term on the right hand side of Eq. (1) represents the change in energy due to the exchange of atoms during defect formation. $\Delta\mu_i$ is the chemical potential of an atom referenced to its bulk, μ_i^{el}. It is a free energy term that can be varied with temperature and pressure, and thus dependent upon growth conditions. In order to maintain stable host under equilibrium, without precipitating the elemental solids we need

$$\Delta\mu_{Sr} + 2\Delta\mu_I = \Delta H(SrI_2), \quad \Delta\mu_{Sr} + \mu^{el}_{Sr} \le \mu^{el}_{Sr}, \text{ and}$$
$$\Delta\mu_I + \mu^{el}_I \le \mu^{el}_I. \tag{A1}$$

The above equation represents the thermodynamic equilibrium of SrI_2 with its constituents. Negative values of $\Delta\mu_i$ expressed in the inequalities avoid the precipitation of the elemental phases. It also signifies that there is a range of possible $\Delta\mu_{Sr}$ and $\Delta\mu_I$ that satisfies this condition. This range may be constricted when we consider dopants and codopants. For example, doping with Eu without forming EuI_2 imposes the additional condition

$$\Delta\mu_{Eu} + 2\Delta\mu_I \le \Delta H(EuI_2). \tag{A2}$$

We can formulate additional condition when a codopant is also present which will restrict formation of relevant competing phases such as MgI_2, BaI_2, CaI_2, SnI_2, SnI_4, CsI, and NaI. These conditions define the boundaries of $\Delta\mu_{Sr}$ and $\Delta\mu_I$. Least negative value of $\Delta\mu_{Sr}$ represents Sr-rich/I-poor condition and vice-versa, as shown in Figs. 3 and 6. The calculated

TABLE II. Calculated formation enthalpy, ΔH of SrI_2, and different competing phases compared with available experimental values at 298 K and 1 bar.[50]

	Formation enthalpy, ΔH (eV/formula unit)		
	PBE	PBE0	Experiment[50]
SrI_2	−4.95	−5.76	−5.78
EuI_2	−5.00	−5.70	…
BaI_2	−5.43	−6.12	−6.24
CaI_2	−4.98	−5.48	−5.53
MgI_2	−3.22	−3.67	−3.77
SnI_2	−1.58	−1.70	−1.19
SnI_4	−1.92	−2.40	−2.15
CsI	…	−3.41	−3.59
NaI	…	−2.88	−2.98

formation enthalpies necessary to determine equilibrium chemical potentials are shown in Table II and compared with available experimental values.

[1]R. Hofstadter, E. O'Dell, and C. Schmidt, IEEE Trans. Nucl. Sci. **11**, 12 (1964).
[2]N. J. Cherepy, G. Hull, A. D. Drobshoff, S. A. Payne, E. V. D. Van Loef, C. M. Wilson, K. S. Shah, U. N. Roy, A. Burger, L. A. Boatner, W-S. Choong, and W. W. Moses, Appl. Phys. Lett. **92**, 083508 (2008).
[3]E. V. D. Van Loef, P. Dorenbos, C. W. E. Van Eijk, K. Kramer, and H. U. Gudel, Appl. Phys. Lett. **79**, 1573 (2001).
[4]M. Nikl, Meas. Sci. Technol. **17**, R37 (2006).
[5]Q. Li, J. Q. Grim, K. B. Ucer, A. Burger, G. A. Bizarri, W. W. Moses, and R. T. Williams, Phys. Status Solidi RRL **6**, 346 (2012).
[6]K. Yang, P. Menge, J. Buzniak, and V. Ouspenski, in *2012 IEEE Nuclear Science Symposium and Medical Imaging Conference (NSS/MIC)* (IEEE, Piscataway, NJ, 2012), pp. 308–311.
[7]M. S. Alekhin, J. T. M. De Haas, I. V. Khodyuk, K. W. Krämer, P. R. Menge, V. Ouspenski, and P. Dorenbos, Appl. Phys. Lett. **102**, 161915 (2013).
[8]K. Nishimoto, Y. Yokota, S. Kurosawa, J. Pejchal, K. Kamada, V. Chani, and A. Yoshikawa, J. Cryst. Growth **401**, 484 (2014).
[9]T. Ito, Y. Yokota, S. Kurosawa, R. Kral, J. Pejchal, Y. Ohashi, K. Kamada, M. Nikl, and A. Yoshikawa, Radiat. Meas. **90**, 157 (2016).
[10]S. Lam, S. E. Swider, A. Datta, and S. Motakef, IEEE Trans. Nucl. Sci. **62**, 3397 (2015).
[11]P. Erhart, B. Sadigh, A. Schleife, and D. Åberg, Phys. Rev. B **91**, 165206 (2015).
[12]P. E. Blöchl, Phys. Rev. B **50**, 17953 (1994).
[13]G. Kresse and J. Hafner, Phys. Rev. B **47**, 558 (1993).
[14]G. Kresse and J. Furthmüller, Comput. Mater. Sci. **6**, 15 (1996).
[15]J. P. Perdew, K. Burke, and M. Ernzerhof, Phys. Rev. Lett. **77**, 3865 (1996).
[16]C. Adamo and V. Barone, J. Chem. Phys. **110**, 6158 (1999).
[17]V. H. Bärnighausen and E. T. Rietschel, Z. Anorg. Allg. Chem. **354**, 23 (1967).
[18]D. J. Singh, Appl. Phys. Lett. **92**, 201908 (2008).
[19]W. Setyawan, R. M. Gaume, R. S. Feigelson, and S. Curtarolo, IEEE Trans. Nucl. Sci. **56**, 2989 (2009).
[20]P. Erhart, A. Schleife, B. Sadigh, and D. Åberg, Phys. Rev. B **89**, 075132 (2014).
[21]V. Pustovarov, I. Ogorodnikov, A. Goloshumova, L. Isaenko, and A. Yelisseyev, Opt. Mater. **34**, 926 (2012).
[22]V. Pankratov, A. Popov, L. Shirmane, A. Kotlov, G. Bizarri, A. Burger, P. Bhattacharya, E. Tupitsyn, E. Rowe, V. Buliga, and R. T. Williams, Radiat. Meas. **56**, 13 (2013).
[23]M.-H. Du and D. J. Singh, Phys. Rev. B **81**, 144114 (2010).
[24]J. Even, L. Pedesseau, J. M. Jancu, and C. J. Katan, J. Phys. Chem. Lett. **4**, 2999 (2013).
[25]W. Känzig, Phys. Rev. **99**, 1890 (1955).
[26]A. L. Shluger and A. M. Stoneham, J. Phys.: Condens. Matter **5**, 3049 (1993).
[27]R. T. Shannon, Acta Cryst. A **32**, 751 (1976).
[28]M. Krings, M. Wessel, and R. Dronskowski, Acta Cryst. C **65**, i66 (2009).
[29]V. H. Bärnighausen and N. Schultz, Acta Crystallogr., Sect. B: Struct. Crystallogr. Cryst. Chem. **25**, 1104 (1969).
[30]A. Chaudhry, R. Boutchko, S. Chourou, G. Zhang, N. Gronbech-Jensen, and A. Canning, Phys. Rev. B **89**, 155105 (2014).
[31]D. H. Gahane, N. S. Kokode, P. L. Muthal, S. M. Dhopte, and S. V. Moharil, Opt. Mater. **32**, 18 (2009).
[32]M. S. Alekhin, J. T. M. de Haas, K. W. Krämer, and P. Dorenbos, IEEE Trans. Nucl. Sci. **58**, 2519 (2011).
[33]Y. Wu, L. A. Boatner, A. C. Lindsey, M. Zhuravleva, S. Jones, J. D. Auxier, H. L. Hall, and C. L. Melcher, Cryst. Growth Des. **15**, 3929 (2015).
[34]B. Kang, C. M. Fang, and K. Biswas, J. Phys. D: Appl. Phys. **49**, 395103 (2016).
[35]C. Freysoldt, B. Grabowski, T. Hickel, J. Neugebauer, G. Kresse, A. Janotti, and C. G. Van de Walle, Rev. Mod. Phys. **86**, 253 (2014).
[36]R. Adhikari, Q. Li, R. T. Williams, A. Burger, and K. Biswas, J. Appl. Phys. **116**, 223703 (2014).
[37]K. Yang and P. R. Menge, J. Appl. Phys. **118**, 213106 (2015).
[38]I. V. Khodyuk, S. A. Messina, T. J. Hayden, E. D. Bourret, and G. A. Bizarri, J. Appl. Phys. **118**, 084901 (2015).
[39]M. A. Brogan, A. J. Blake, C. Wilson, and D. H. Gregory, Acta Cryst. C **59**, i136 (2003).
[40]T. Koopmans, Physica **1**, 104 (1934).
[41]Q. Li, R. T. Williams, and D. Åberg, Phys. Status Solidi B **250**, 233 (2013).
[42]H. Shi and M.-H. Du, Phys. Rev. B **90**, 174103 (2014).
[43]S. A. Payne, N. J. Cherepy, G. Hull, J. D. Valentine, W. W. Moses, and W.-S. Choong, IEEE Trans. Nucl. Sci. **56**, 2506 (2009).
[44]J. Q. Grim, K. B. Ucer, A. Burger, P. Bhattacharya, E. Tupitsyn, E. Rowe, V. M. Buliga, L. Trefilova, A. Gektin, G. A. Bizarri, W. W. Moses, and R. T. Williams, Phys. Rev. B **87**, 125117 (2013).
[45]K. B. Ucer, G. Bizarri, A. Burger, A. Gektin, L. Trefilova, and R. T. Williams, Phys. Rev. B **89**, 165112 (2014).
[46]K. Biswas and M.-H. Du, Phys Rev. B **86**, 014102 (2012).
[47]F. Zhou, B. Sadigh, P. Erhart, and D. Åberg, NPJ Comput. Mater. **2**, 16022 (2016).
[48]S. Lany and A. Zunger, Phys. Rev. B **78**, 235104 (2008).
[49]G. Makov and M. C. Payne, Phys. Rev. B **51**, 4014 (1995).
[50]*CRC Handbook of Chemistry and Physics*, edited by D. R. Lide (Boca Raton, FL, 2000).